Langmuir

Article

pubs.acs.org/Langmuir

Monte Carlo Modeling of Carbon Dioxide Adsorption in Porous Aromatic Frameworks

Alberto Fraccarollo, Lorenzo Canti, Leonardo Marchese, and Maurizio Cossi*

Dipartimento di Scienze e Innovazione Tecnologica (DISIT), Centro Interdisciplinare Nano-SiSTeMI, Università del Piemonte Orientale, via T. Michel 11, I-15121, Alessandria, Italy

Supporting Information

ABSTRACT: The adsorption isotherms of CO_2 in several porous aromatic frameworks (PAFs) have been simulated with Grand Canonical Monte Carlo technique, to support the synthesis of new materials for efficient carbon dioxide capture and storage. The simulations covered the 0−60 bar pressure range and were repeated at 273, 298, and 323 K. The force field employed in the simulations was optimized to fit the correct behavior of the free gas and to reproduce the CO_2−phenyl interactions computed at high quantum mechanical level. PAFs are based on the diamond structure, with polyaromatic chains inserted in C−C bonds. We examined four PAF-30*n* (*n* being the number of phenyl rings in the aromatic linkers), finding that PAF-302 is overall the best performing, although PAF-301 provides higher adsorbed densities at very low pressure. The CO_2 adsorption then was simulated in a number of modified PAF-302, with different functional groups (amino-methane, toluene, pyridine, and imidazole) attached to the phenyl chains; different degrees of substitution (25%, 50%, and 100% derivatized rings) were considered. The effects of functionalization and the dependence on the substitution degree are carefully discussed, to determine the most promising materials at low, intermediate, and high pressures.

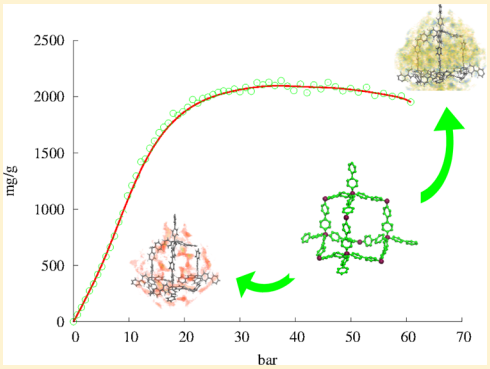

1. INTRODUCTION

The ever-growing energy demand, largely satisfied by the combustion of fossil fuels, caused an escalated global CO_2 emission, which became the major cause of global warming. Besides the attempts to reduce anthropogenic emissions, it has been proposed to control atmospheric CO_2 concentration removing the gas from the air through carbon capture and storage (CCS) techniques, whose study is strongly supported by governments and scientific institutes.[1,2]

In CCS technology, the adsorption in microporous materials has been considered recently for its economic and environmental advantages. Nanoporous dipeptide-based materials,[3] carbon-based materials,[4,5] zeolites,[6] metal−organic frameworks (MOFs),[7−9] covalent−organic frameworks (COFs),[10] zeolitic imidazolate frameworks (ZIFs),[11] and porous aromatic frameworks (PAFs)[12] are being considered as candidates to capture CO_2. The performance of a very large number of porous solids, mainly zeolites and MOFs, have also been compared computationally with a specific protocol, to predict the energy demand and efficiency in actual plants.[13] Covalent−organic frameworks were also modeled with a variety of approaches,[14] including the so-called connectivity-based atom contribution method[15] and force fields derived from quantum-mechanical calculations (at the DFT and MP2 levels).[16]

Among the newest materials, PAFs are raising a great interest as adsorbent materials, due to their very low density, large surface area, high porosity, exceptional structural properties, and high thermal and hydrothermal stability.[12,17−20] Here, we consider different members of the PAF family, collectively indicated as PAF-30*n* (where $n = 1−4$ is the number of phenyl rings inserted in the C−C bonds of the diamond structure; see below).[21] Among this series, only PAF-302, sometimes referred to as PAF-1 in the literature, has been synthesized and characterized so far, although several variants and functionalizations of the original PAF-302 have been studied.[22−27] Note that, although Trewin and Cooper suggested the PAF-302 might be amorphous based on the powder X-ray diffraction pattern,[28] all of the model studies about its adsorption properties were based on a crystalline structure.

In their original work, Ben and co-workers proposed a method to synthesize the first high surface area PAF with *dia* topology (i.e., PAF-302, therein called PAF-1),[12] via a nickel(0)-catalyzed Yamamoto-type Ullmann cross-coupling. The resulting crystalline material showed a record specific surface area (SSA, 5640 m^2/g with BET method) and an exceptional physicochemical stability; furthermore, it provided a very high uptake of carbon dioxide (1.3 g/g at 40 bar, 298 K). Recently, the record for SSA was gained by another porous aromatic polymer network, PPN-4,[29] with BET SSA as high as 6463 m^2/g. Continuining their research, Ben and co-workers

Received: January 28, 2014
Revised: March 18, 2014
Published: March 19, 2014

   dx.doi.org/10.1021/la500111a | *Langmuir* 2014, 30, 4147−4156

have proposed in 2013 new carbonized PAF-302 derivatives formed by high-temperature KOH activation, which show a bimodal microporous structure with pores of 0.6 and 1.2 nm width and specific surface area in the range 1000−3000 m^2/g; carbon dioxide, methane, and hydrogen sorption experiments indicated that these novel porous carbon materials perform very well both in low- and in high-pressure ranges.[23]

Still, in 2013 Yang et al. have systematically investigated the CO_2 storage in PAFs with molecular simulations,[30] finding that the first member of the series (PAF-301), due to its small pore size, exhibits a very high CO_2 uptake at low pressure (275 mg/g at 298 K and 1 bar) along with much higher selectivities for the CO_2/H_2, CO_2/N_2, CO_2/CH_4, and CH_4/H_2 mixtures than the other PAFs. The CO_2 uptake in PAF-302, -303, and -304 was predicted at 1850, 3432, and 3124 mg/g (298 K and 50 bar), respectively, thus larger than MOF-200 (2437 mg/g) and MOF-210 (2396 mg/g), suggesting that PAFs have a very high affinity for CO_2. Note that gravimetric uptakes are strongly favored in materials with very low densities, while the order can change when considering volumetric adsorption. For instance, using PAF theoretical densities reported in ref 30, the volumetric CO_2 uptakes at 50 bar are 583, 553, and 312 mg/cm^3 for PAF-302, -303, and -304, respectively; of course, theoretical densities refer to those of ideal materials and can be quite different from the measured densities of actual adsorbers.

In this Article, we perform Grand Canonical Monte Carlo (GCMC) simulations to explore the ability of several members of the PAF family to adsorb gaseous carbon dioxide at pressures ranging from 0 to ca. 60 bar and temperatures of 273, 298, and 353 K. From one side, we want to assess the performances of PAFs with a rigorous derivation of force fields, specifically optimized for the systems in exam; in fact, reliable theoretical predictions referring to ideal, crystalline systems can be of great help in the synthetic work, providing upper bounds for experimental adsorptions, serving as benchmarks to evaluate the goodness of materials actually synthesized, and assisting the interpretation of experimental results. Furthermore, we investigate at the same level the CO_2 adsorption in a large group of functionalized PAF-302, varying the nature and the concentration of functional groups, to suggest the best candidates for highest carbon dioxide capture and storage. A number of data, collected in tables and figures, are also reported in the Supporting Information.

2. METHODS

2.1. Calculation Level. Monte Carlo simulations of adsorption and linear energy scans were performed with the Sorption and Forcite modules of Materials Studio suite,[31,32] respectively; for structure optimizations, the COMPASS26 force field (FF) was used, while for GCMC calculations we adopted a modified version of Dreiding FF (see below). Ab initio calculations for structure optimizations were performed at the DFT level with B3LYP[33] functional and 6-31+G(d,p)[34,35] basis set using the program CRYSTAL09,[36] while single-point energy calculations were performed at the MP2 level with 6-311+G(2d,2p) basis set, including the counterpoise correction of the Basis Set Superposition Error (BSSE),[37] with the Gaussian 09 program.[38]

2.2. Fugacity Coefficients. The key quantity in GCMC simulations is the chemical potential, depending on temperature and fugacity. To compare GCMC results with experimental measures, one has to convert fugacities into pressures, in the entire pressure range of interest. The distinction between fugacities and pressures, sometimes neglected in the literature on simulated adsorptions, is particularly important when high pressures are reached as in the present case. We computed the CO_2 fugacity coefficients $\phi(P,T)$ at the desired conditions through the formula:

$$\phi(P, T) = \int_0^P \frac{Z(P', T) - 1}{P'} \, dP' \quad (1)$$

where Z is the compression factor, obtained from the experimental molar volumes of gaseous carbon dioxide at 273, 298, and 323 K. The data at the various temperatures and pressures were taken from ref 39, and based on the equation of state reported in ref 40.

3. MODELS OF PAFs

PAF-30*n* materials are based on diamond structure, with *n* phenyl rings inserted in each C−C bond (Supporting I, Figure S1), as described, for example, in the seminal paper by Ben et al.[12] We adopted the procedure described in detail in our previous work about methane adsorption[41] to build periodic models of PAF-30*n*, $n = 1-4$, with the difference that in the present work the unit cell parameters and atomic coordinates were optimized for all of the systems. PAF-301 and PAF-302 optimizations were performed at the DFT level with the CRYSTAL09 program, while PAF-303 and PAF-304, due to the large size of their unit cells, were optimized with the Materials Studio Forcite module and COMPASS26 force field.

Although PAFs are relatively new materials, their performance in gas adsorption has been deeply studied with various techniques. Some works have pointed out that the adsorption of methane, hydrogen, and CO_2 can be enhanced by a suitable derivatization of the parent PAF-302 (the only member of the PAF-30*n* family actually synthesized so far). The proposed functionalizations include the postsynthesis lithiation, the treatment with sulfonic acid/lithium sulfonate, and also the carbonization (possibly with KOH activation); the last approach leads to a partial collapse of the PAF structure with the formation of ultramicropores besides the usual PAF-302 micropores. The best results, at least at low pressure, were obtained in PAF-302 functionalized with NH_2-CH_2- moieties;[42] besides, recent calculations predicted that the addition of polar moieties (tetrahydrofuran-like rings fused with the biphenyl rings) should improve the gas loading markedly.[22] In addition, a rich literature exists about the effect of functionalized ligands on CO_2 adsorption in metal−organic frameworks, which has evidenced the very promising effects of aromatic and amino-aromatic moieties, thanks to enhanced polar interactions.[43,44]

Therefore, we decided to simulate the adsorption in several modified PAF-302, first adding aminomethyl and tolyl groups, then using other moieties that somehow combine these functional groups, including imidazole (Imi) and pyrimidine (Pyr). The complete list of functional groups is reported in Figure 1. Besides the nature of the attached group, the degree of functionalization is also an important parameter. PAF-302 is usually synthesized by Yamamoto coupling from tetrakis(*p*-bromophenyl)methane, so that when one, two, or four phenyl rings are derivatized in the reactant, one obtains functional PAF-302 with 25%, 50%, or 100% modified aromatic rings, respectively, as shown in Figure 2. Because the PAF-302 unit cell contains 16 biphenyl linkers, R-PAF(25%), (50%), and (100%) have 8, 16, and 32 functional groups in the unit cell, respectively.

The unit cell parameters and the atomic coordinates for all of the substituted PAF-302 were optimized with the Materials Studio Forcite module.

dx.doi.org/10.1021/la500111a | Langmuir 2014, 30, 4147−4156

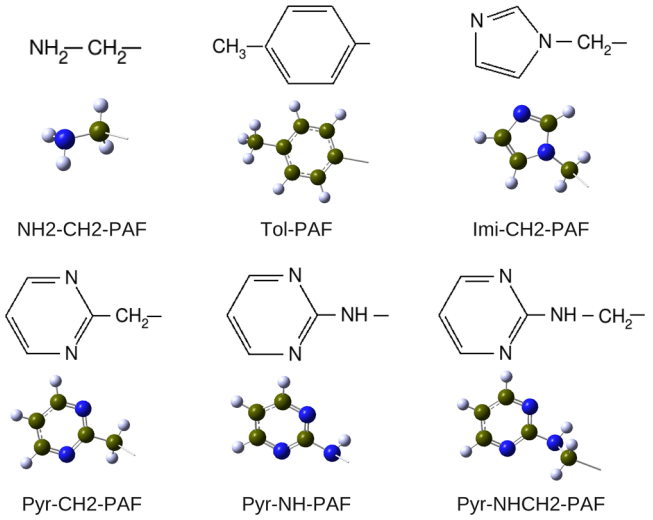

Figure 1. Functional groups attached to biphenyl chains in PAF-302. Lewis structure, ball-and-stick model, and name of the corresponding functionalized PAF-302 are indicated for each group.

Some structural properties, requiring a measure of the skeletal density of the simulated materials, were estimated using the GEPOL procedure,[45] implemented in Gaussian 09 as a part of the Polarizable Continuum Model of solvation.[46] GEPOL approximates the molecular volume and surface with the envelope of spheres centered on the atoms, and provides a realistic description of the actual molecular shape and size. In the present work, we used atomic radii of 1.7, 1.2, and 1.5 Å for C, H, and N atoms, respectively. The structural data for all of the optimized simulated materials are listed in Table S1 (Supporting Information).

4. FORCE FIELD PARAMETRIZATION

For our simulations, we modified the Dreiding Force Field (FF),[47] which is widely used to simulate intermolecular host–guest interactions; for instance, it was recently used without changes to predict gas adsorption in MOFs and COFs materials.[48] In this FF, noncovalent interactions between molecules A and B are described with a combination of pairwise Lennard-Jones (LJ) and Coulombic potentials:

$$U_{AB} = \sum_{\substack{\alpha\in A\\ \beta\in B}} \left\{ 4D_{\alpha\beta}\left[\left(\frac{\sigma_{\alpha\beta}}{r_{\alpha\beta}}\right)^{12} - \left(\frac{\sigma_{\alpha\beta}}{r_{\alpha\beta}}\right)^{6}\right] + \frac{q_\alpha q_\beta}{4\pi\varepsilon_0 r_{\alpha\beta}} \right\} \quad (2)$$

$$D_{\alpha\beta} = (D_\alpha \cdot D_\beta)^{1/2} \quad (3)$$

$$\sigma_{\alpha\beta} = \frac{1}{2}(\sigma_\alpha + \sigma_\beta) \quad (4)$$

where α and β indicate the atoms separated by distance r, q is the atomic fractional charge, and D and σ are the well depth and the collision diameter of the pairwise LJ potential, respectively, defined in terms of atomic parameters.

The FF was tested first for gaseous CO_2, simulating a formal "adsorption" in an empty box and computing the compressed gas density at 298 K. The results were compared with the experimental data;[39,40] carbon and oxygen partial charges were estimated with the Mulliken method from a MP2 calculation on isolated CO_2 molecule and kept unaltered in all of the simulations. As shown in Figure S2 (Supporting Information), the standard FF provides densities somehow too low, so that the Lennard-Jones parameters for carboxylic C and O (C_1 and O_2 in Dreiding notation, respectively) were slightly modified to make it more attractive. The reliability of the new parameters was also confirmed by comparing the trend of CO_2–CO_2 intermolecular energies computed by Forcite with the modified

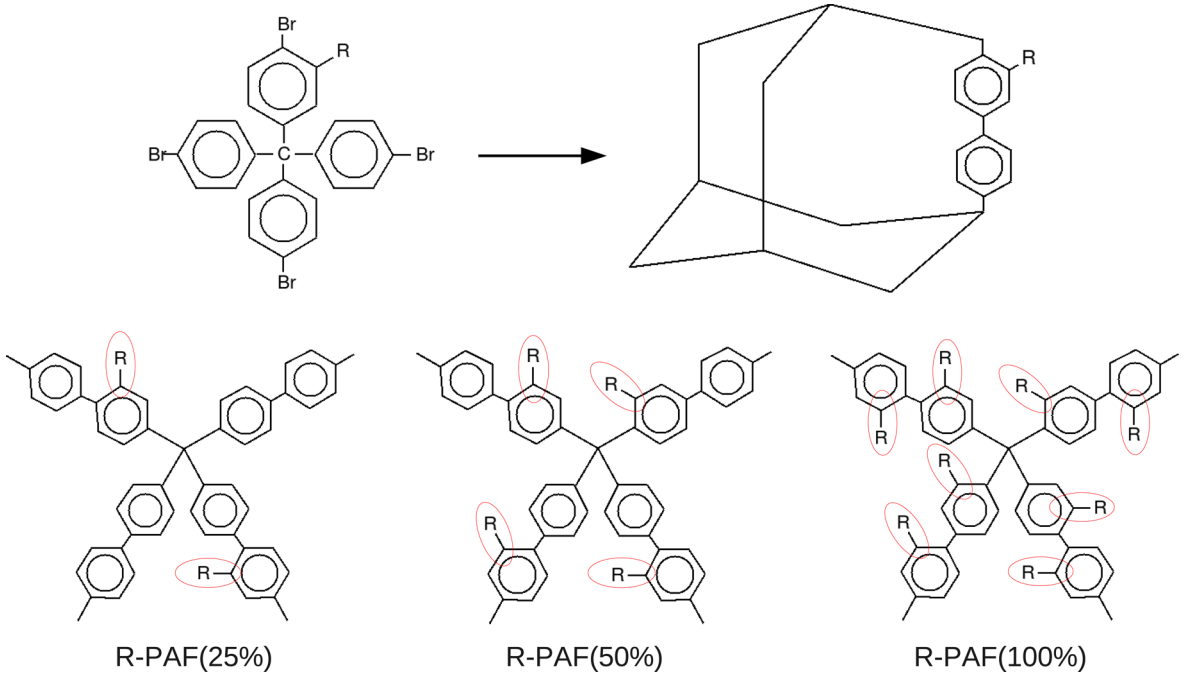

Figure 2. Top: A singly substituted tetrakis(*p*-bromophenyl)methane giving rise to PAF-302 with one functional group per biphenyl chain, on average. Bottom: Scheme of derivatized PAF-302 lattice with one-fourth (25%), one-half (50%), and all (100%) phenyl rings bearing a functional group.

dx.doi.org/10.1021/la500111a | *Langmuir* 2014, 30, 4147–4156

FF and by Gaussian 09 at the MP2 level, with correction of the BSSE, along two different orientations, as shown in Figure S3 (Supporting Information).

Host−guest interactions were considered next, comparing classical and MP2 intermolecular energies for the CO_2−benzene couple along different orientations. Because Mulliken charges for the aromatic moiety were markedly unstable and orientation-dependent, we chose to set aromatic carbon and hydrogen partial charges to zero, and only use Lennard-Jones parameters for computing host−guest interactions. Keeping C_1 and O_2 parameters previously optimized, the LJ parameters for aromatic carbon (C_R in Dreiding notation) were adjusted to obtain a satisfatory fit of classical and ab initio curves, as reported in Figure S4 (Supporting Information). With the same procedure, we verified that this FF also reproduces well the CO_2−toluene interactions (Figure S5, Supporting Information).

Finally, we dealt with functionalized PAF-302 containing amino and heterocyclic groups. Classical and MP2 energies were compared for CO_2 interacting with phenyl−CH_2−R (R = NH_2, imidazole, pyrimidine), with the results shown in Figures S6−S8 (Supporting Information). In this case, the LJ parameters for amino N and H and for heterocyclic (aromatic) N were modified to obtain a satisfactory agreement. All of the modified parameters are listed in Table S2 (Supporting Information).

5. RESULTS

5.1. Simulated Adsorption Isotherms in PAF-30*n*. The GCMC simulated adsorption isotherms at 298 K, along with the density of the free gas at the same pressures, are reported in Figure 3. One can see that all of the considered materials

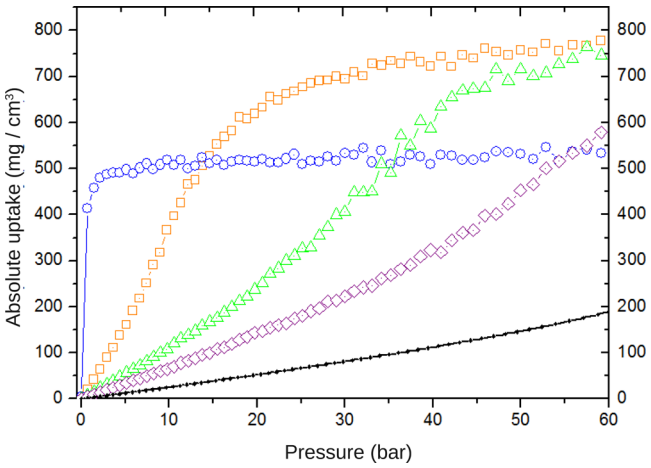

Figure 3. CO_2 adsorbed density (absolute volumetric adsorption, mg/cm^3) at 298 K. Blue ○, PAF-301; orange □, PAF-302; green △, PAF-303; purple ◇, PAF-304; ●, experimental density of the compressed gas.

adsorb carbon dioxide very efficiently at low and high pressure. PAF-302 exhibits the best behavior, except in the initial step (P < 15 bar) where PAF-301 performs better, likely due to the smaller pore size (with an average pore diameter of 7−8 Å, PAF-301 is close to the boundary between micro- and ultramicroporous materials), which amplifies the host−guest interactions but leads to a faster saturation.

Overall PAF-302, as already shown in previous studies,[41] presents the best combination of large surface area and microporosity. Figure 3 reports the absolute adsorption isotherms, that is, the gas density that would be stored in a container filled by the adsorbent; in the experimental literature, other related quantities are often encountered:

$$n_{exc} = n_{ads} - f_{pore} \times \rho_{free} \quad (5)$$

$$n_{eff} = n_{ads} - \rho_{free} \quad (6)$$

where n_{ads}, n_{exc}, and n_{eff} are the absolute, excess, and effective adsorbed densities, respectively, ρ_{free} is the free gas density (continuous line in Figure 3), and f_{pore} is the material porous fraction (see Table S1 in the Supporting Information).

Simulated excess and effective adsorptions for PAF-30*n* at 298 K are reported in Figure S9 (Supporting Information). At this temperature, the largest gain with respect to the compressed gas is obtained with PAF-302, whose maximum n_{eff} occurs at 37.4 bar, where the storage density is increased from 84.0 to 659.4 mg/cm^3 with a gain factor of 7.8 with respect to the free gas. The storage density is enhanced by the other materials too, although to a lesser extent: maximum n_{eff} occurs at 9.8, 45.9, and 59.1 bar for PAF-301 (gain factor 28.5), PAF-303 (5.3), and PAF-304 (2.5), respectively. At the largest pressure considered, 60.8 bar, the carbon dioxide density in PAF-302 is still more than 3 times the corresponding free gas density (579.1 vs 191.4 mg/cm^3).

The temperature effect on CO_2 adsorption was evaluated by repeating the simulations at 273 and 323 K on all of the PAF-30*n*; the corresponding absolute, excess, and effective isotherms are shown in Figures S10−S12 (Supporting Information). The adsorption is greatly influenced by the temperature, especially at low pressures; for instance, at 14.2 bar the adsorbed density in PAF-302 passes from 727.9 mg/cm^3 at 273 K to 528 mg/cm^3 at 298 K, to 297.9 mg/cm^3 at 323 K.

Recently, the carbon dioxide adsorption in PAF-302 has been studied experimentally both at 273 and at 298 K.[12,18,42] In Figure 4, we compare these measured adsorbed densities with our volumetric theoretical predictions. The comparison between the corresponding gravimetric curves is reported in Figure S13 (Supporting Information). Simulated and experimental isotherms are in good agreement at low pressure, and show increasing discrepancies at higher pressures. Such differences are likely due to the ideal crystalline structure of the model PAF-302, in contrast to the probable presence of defects in the real samples. In fact, an incomplete or defective polymerization during PAF synthesis can lead to a smaller active area, and to a partial obstruction of pores; because crystalline PAF-302 seems to be ideally suited for gas adsorption, as noted above, any modification of the structure is likely to lower the uptake, especially at high pressure.

It is also interesting to compare our simulations to Yang et al.'s theoretical results,[30] already mentioned in the Introduction. At 50 bar and 298 K, our computed CO_2 uptakes are systematically larger: 750 versus 583 mg/cm^3 for PAF-302, 700 versus 553 mg/cm^3 for PAF-303, and 450 versus 312 mg/cm^3 for PAF-304. Actually, in ref 30 the force field was chosen to fit the experimental CO_2 uptake in PAF-302 reported by Ben et al.;[12] the present force field, on the contrary, was modified as explained above to fit experimental guest−guest and ab initio host−guest interaction energies. We have just commented the discrepancies with the experimental uptakes in terms of nonideality of the actual samples; in our view, GCMC

dx.doi.org/10.1021/la500111a | Langmuir 2014, 30, 4147−4156

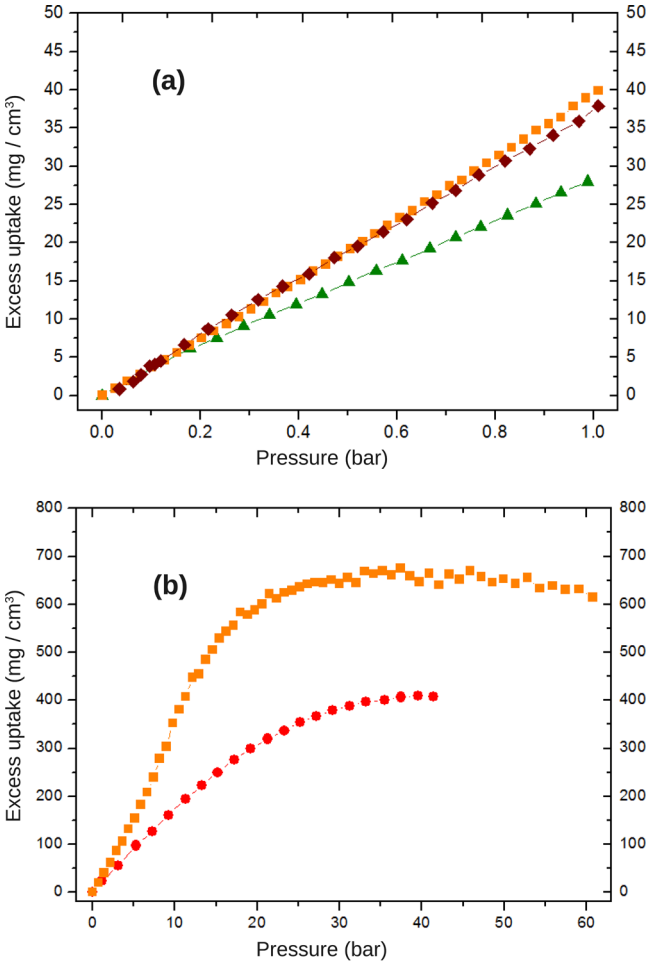

Figure 4. Simulated and experimental volumetric CO_2 adsorption in PAF-302 at 273 K, at low (a) and high (b) pressure. Orange ■, this work; purple ◆, ref 42; green ▲, ref 18; red ●, ref 12.

simulations on "perfect" PAF crystals can be considered as upper bounds for the adsorption behavior of real materials, provided reliable force fields are used.

More results have been obtained for the CO_2 adsorption in other porous materials, including metal organic frameworks (MOF) and covalent organic frameworks (COF), as shown in Table 1, where gravimetric uptakes (e.g., weight % or milligrams of gas adsorbed per gram of material) are reported for some of the best performing materials. Note that, as

Table 1. CO_2 Excess Gravimetric Uptake in Different Materials

material	conditions	CO_2 excess uptake (mg/g)	ref
MOF-200	50 bar, 298 K	2437	7
MOF-210	50 bar, 298 K	2396	7
COF-102	55 bar, 298 K	1200	53
COF-103	55 bar, 298 K	1190	53
NJU-Bai12	20 bar, 298 K	873	54
K-PAF-1[a]	1 bar, 273 K	352	23
K-PAF-1[a]	40 bar, 273 K	1300	23
	1.4 bar, 298 K	128	
PAF-302	20 bar, 298 K	1905	this work
	50 bar, 298 K	2072	

[a]Carbonized PAF-302 with KOH activation.

remarked above, gravimetric data are easier to obtain but somehow misleading, because the lightest materials are favored in the comparison: volumetric uptakes are more directly comparable, as they depend on the actual porosity and specific surface area of the materials. Keeping in mind this limitation, the data in Table 1 clearly show that PAF-302 can be an exceptional adsorber for CO_2; for instance, its excess uptake at 298 K and 50 bar in PAF-302 is predicted to be as high as 2072 mg/g, among the best results reported so far. This is even more appealing if one takes into account the high thermal and hydrothermal stability exhibited by PAFs; the stability in the presence of humidity has been an issue for many high surface area adsorbent materials, like the first synthesized MOFs,[49,50] although recent advances led to the preparation of water-stable metal organic frameworks, too.[51,52]

5.2. Isosteric Heat. The ability of a material as a gas adsorber depends on the interactions that establish between the gaseous molecules and the material surface, mainly inside the pores. Such ability is effectively measured by the adsorption enthalpy change, also called isosteric heat of adsorption (Q_{st}), which can be obtained through the Clausius−Clapeyron equation at different gas uptakes:

$$Q_{st} = -\Delta\bar{H}_{ads} = -R\left(\frac{\partial \ln f}{\partial(1/T)}\right)_{n_{exc}} \quad (7)$$

where n_{exc} is the excess adsorbed density and f is the fugacity of the free gas in equilibrium with n_{exc}. Note that excess isotherms indicate the quantity of gas that is adsorbed as a consequence of gas−surface interactions, thus exceeding the gas that would be stored inside the pores if no interactions were present, and this is directly related to Q_{st}. In practice, the simulations were repeated at 273, 298, and 323 K; at different temperatures, different values of free gas fugacities were needed to obtain the same n_{exc}. Q_{st} then was computed as the slope of the line fitting the values of $\ln(f)$ versus $1/T$, for each selected value of n_{exc}.

In Figure S14 (Supporting Information), the isosteric heat is reported as a function of the gas loading for PAF-302, 303, and 304 (PAF-301 saturates so quickly at low pressure that it is difficult to obtain reliable data at different temperatures). The three materials exhibit very similar Q_{st} values up to an excess loading of about 40 mg/cm^3, reflecting the similarity in the gas/surface interactions. PAF-302 heat is slightly larger, however, likely due to the possibility for single gas molecules to interact with two aromatic rings bonded to the same aliphatic carbon at a favorable angle (see Supporting Information Figure S14, inset); this possibility is comparatively smaller in PAF-303 and 304, which contain longer, linear polyphenyl chains.

Simulated Q_{st} for PAF-302 can also be compared to experimental values. Figure S15 (Supporting Information) shows that our model is in very good agreement with the measures reported by Ben and co-workers in ref 12. In Supporting Information Figure S15, we also report the somehow underestimated isosteric heat computed by Yang et al.;[30] as already discussed above, the FF used in ref 30 is less attractive than our FF, leading to smaller values for Q_{st}. Note that the experimental gas uptake measured in ref 12 at high pressure is markedly lower than our simulation, as shown in Figure 4b. As commented above, the discrepancy is likely due to the crystalline structure of the real sample, while the agreement in isosteric heats at small pressure confirms the reliability of the energetic interactions computed by the present model.

dx.doi.org/10.1021/la500111a | Langmuir 2014, 30, 4147−4156

5.3. Simulated Adsorption Isotherms in Functionalized PAF-302. As was already noted, suitable functionalizations are expected to increase the CO_2 adsorption in PAF markedly, at least at low pressure. In the following, the simulated adsorption isotherms are discussed for the modified PAF-302 models described above. The gas loadings at 298 K at low pressure (up to 1 bar) and for the whole pressure range (up to 60 bar) are reported in Figures 5 and 6, respectively, for all

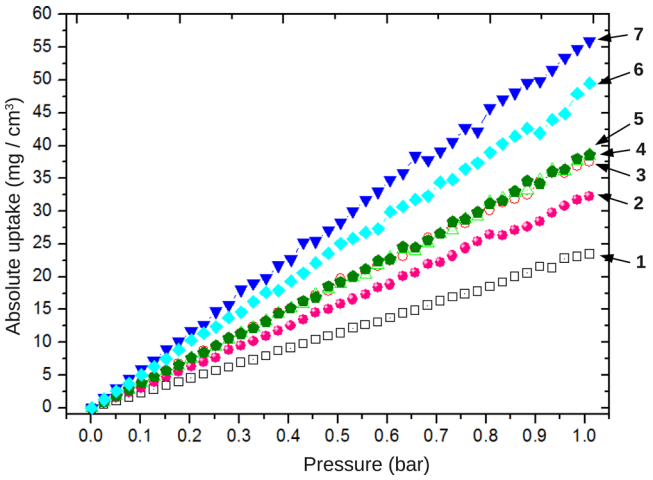

Figure 5. CO_2 adsorbed density (absolute volumetric adsorption, mg/cm^3) in functionalized PAF-302 at 298 K, with 25% substitution. 1, unmodified PAF-302; 2, Imi-CH2-PAF; 3, NH2-CH2-PAF; 4, Tol-PAF; 5, Pyr-CH2-PAF; 6, Pyr-NHCH2-PAF; 7, Pyr-NH-PAF.

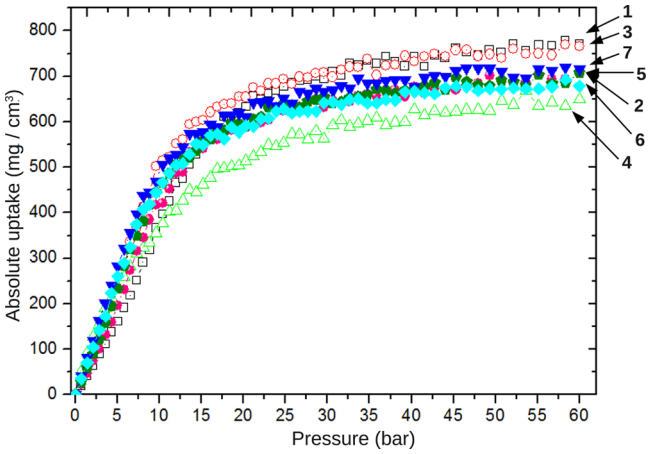

Figure 6. CO_2 adsorbed density (absolute volumetric adsorption, mg/cm^3) in functionalized PAF-302 at 298 K, with 25% substitution. 1, unmodified PAF-302; 2, Imi-CH2-PAF; 3, NH2-CH2-PAF; 4, Tol-PAF; 5, Pyr-CH2-PAF; 6, Pyr-NHCH2-PAF; 7, Pyr-NH-PAF.

of the functionalized PAF-302 with 25% substitution degree (i.e., with 8 functional groups per unit cell); the curves for the unmodified PAF-302 are also shown for comparison. The corresponding gravimetric curves (expressing the gas loading in mg/g units) are also reported in Figures S16, S17 (Supporting Information). Because of the different densities of the materials (see Supporting Information Table S1), gravimetric and volumetric isotherms have somehow different aspects, although the order of loadings is the same.

At low pressure, all of the functionalized materials perform much better than PAF-302. The highest loading is recorded for Pyr-NH-PAF whose adsorption at 1 bar is more than 2.5 times higher than in the unmodified system. The second and third best performances are provided by Pyr-NHCH2-PAF and Pyr-CH2-PAF (with loadings 2.25 and 1.75 times higher than in PAF-302, respectively, at 1 bar), clearly indicating that pyrimidine is the most promising functional group for this kind of application. Tolyl and aminomethyl groups enhance the adsorption to a good extent, too, proving almost as efficient as Pyr-CH2-PAF in this pressure range; on the other hand, imidazole group provides quite a poor performance. Note that in the gravimetric plot (Supporting Information Figure S16), NH2-CH2-PAF performs quite better than Tol- and Pyr-CH2-PAF, thanks to its lower density.

The picture is quite different when high pressures are considered. In Figure 6, the isotherms are closer to each other, but the best performing material in this case is the unmodified PAF-302 followed by NH2-CH2-PAF, the worst being Tol-PAF. Apparently at higher pressure, when the adsorbed gas density grows, the available porous volume becomes more important than the strength of gas−surface interactions, which predominates at low pressure. Indeed, PAF-302 and NH2-CH2-PAF have the largest specific porous volume in the series, that is, 2.58 and 2.25 cm^3/g, while none of the other materials exceeds 1.90 cm^3/g (Supporting Information Table S1).

In Figure 7, the simulated excess adsorptions in NH2-CH2-PAF are compared to the experimental results presented in ref

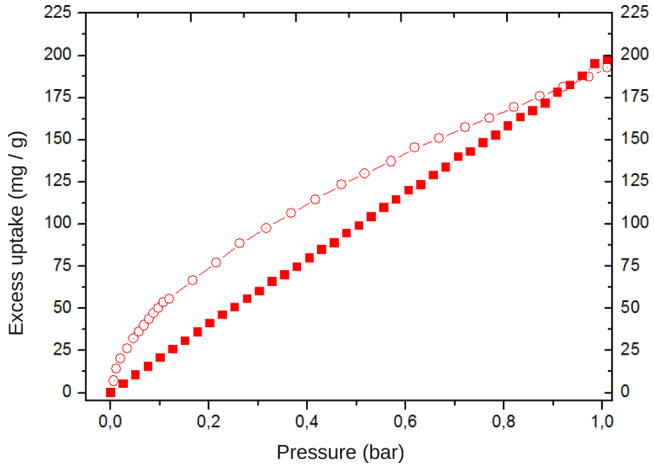

Figure 7. Simulated and experimental CO_2 gravimetric adsorbed density (mg/g) in NH2-CH2-PAF(25%) at 273 K. Red ■, Monte Carlo simulation, this work; red ○, ref 42.

42 (note that both experimental and theoretical data in this figure are obtained at 273 K). The agreement is quite good, although the measured isotherm grows more steeply at very low pressure, and starts bending as in near-saturation regime at 1 bar, while the simulated curve is almost linear in this pressure range (it bends markedly around 15 bar; see Figure 6). The former behavior is quite typical of ultramicroporous materials, as seen for instance in the simulated isotherms in PAF-301 (Figure 3), and it could be explained by an imperfect polymerization leading to a lower porous volume than in the ideal crystalline material. Indeed, the NH2-CH2-PAF BET surface area measured in ref 42 is 1363 m^2/g (to be compared to 4100 m^2/g for the starting PAF-302), with a corresponding reduction of the porous volume from 2.73 to 0.74 cm^3/g and a 2 Å decrease of the dominant pore diameter. Comparing this data with the ideal structural properties listed in Table S1 (Supporting Information), one can see that the changes cannot

dx.doi.org/10.1021/la500111a | Langmuir 2014, 30, 4147−4156

be explained simply by the steric hindrance of the added functional group, but they are likely due to a partial collapse of the crystalline structure.

Increasing the degree of functionalization (i.e., passing to materials with 16 and 32 functional groups per unit cell), one obtains the adsorption isotherms shown in Figures 8 (pressure up to 1 bar) and 9 (pressure up to 60 bar). Imi-CH2-PAF and Pyr-CH2-PAF were not included in these simulations, which are very expensive computationally, the former for its poor performance in the 25% substituted material, the latter because it was the less satisfactory among the pyrimidine derivatives.

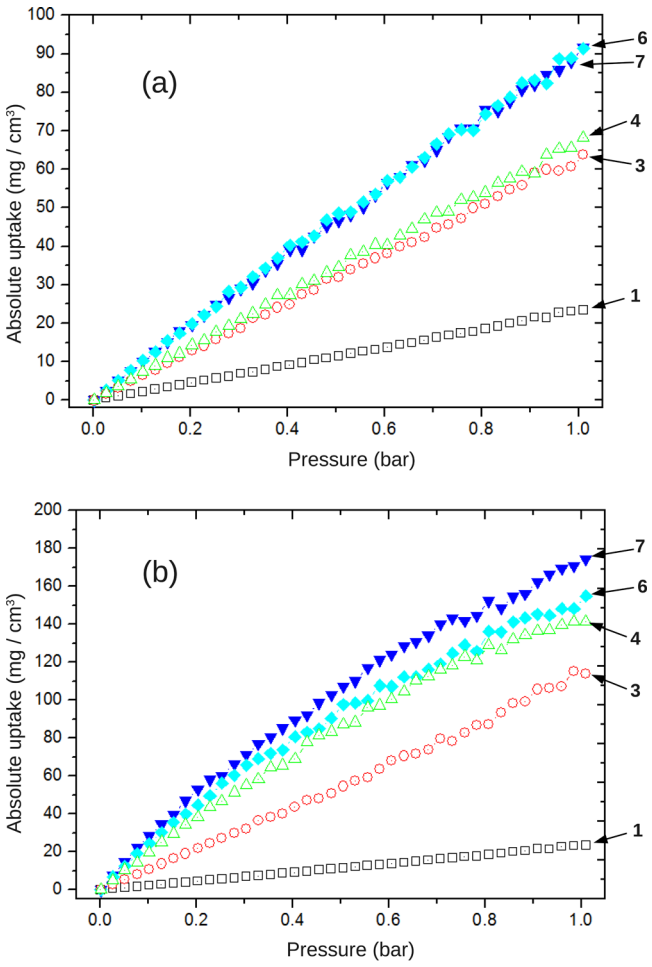

Figure 8. CO_2 adsorbed density (absolute volumetric adsorption, mg/cm^3) in functionalized PAF-302 at 298 K, with (a) 50% substitution, and (b) 100% substitution. 1, unmodified PAF-302; 3, NH2-CH2-PAF; 4, Tol-PAF; 6, Pyr-NHCH2-PAF; 7, Pyr-NH-PAF.

The trends in the highly functionalized materials are very interesting. At low pressure the CO_2 uptake is dramatically higher than in standard PAF-302. With 50% functionalization degree, Pyr-NHCH2-PAF and Pyr-NH-PAF adsorb up to 6.7 times more gas than PAF-302, reaching an adsorbed density of 187 mg/cm^3 at 1 bar, while NH2-CH2-PAF and Tol-PAF present a gain factor of about 4.6. In the 100% derivatized material (Figure 8b), the trend is even more evident, with uptakes 8.5−10.5 times higher than in PAF-302. At 1 bar the best performing material is Pyr-NH-PAF(100%), which adsorbs 305 mg/cm^3, although its isotherm shows a near-saturation bending.

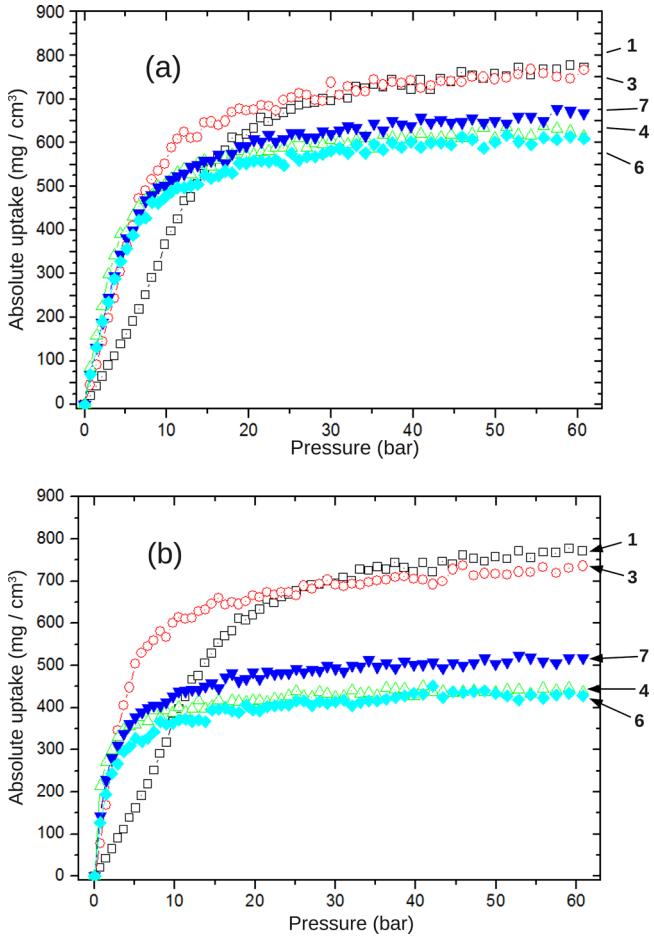

Figure 9. CO_2 adsorbed density (absolute volumetric adsorption, mg/cm^3) in functionalized PAF-302 at 298 K, with (a) 50% substitution, and (b) 100% substitution. 1, unmodified PAF-302; 3, NH2-CH2-PAF; 4, Tol-PAF; 6, Pyr-NHCH2-PAF; 7, Pyr-NH-PAF.

As was already observed, at higher pressures the porous volume becomes determinant, and above 25 bar the unmodified PAF-302 is able to adsorb more gas than the functionalized counterparts, both at 50% and at 100% substitution degree. NH2-CH2-PAF, however, performs almost equally well at high pressure, besides being clearly more efficient than PAF-302 at intermediate pressure (1−20 bar). This is likely due to a good combination of enhanced gas−surface interactions and still large porous volume.

It is also worth examining the gravimetric adsorption isotherms reported in Figures S18, S19 (Supporting Information); especially for the fully derivatized materials, whose density is higher of course, there are evident differences with respect to the volumetric isotherms discussed above. For instance, NH2-CH2-PAF(100%) is largely the best adsorbent at 1 bar, outperforming Pyr-NHCH2-PAF(100%), which was the most efficient in the volumetric plot but is unfavored by its much higher density. On the other hand, at high pressure the gravimetric uptakes of NH2-CH2-PAF(50%) and NH2-CH2-PAF(100%) are markedly lower than in PAF-302, while they were comparable in the volumetric plots. In this case indeed, the functionalized material is more dense than the unmodified solid. Whether gravimetric or volumetric plots are more useful to compare materials performance depends to a great extent on the sought applications. Because PAFs, as well as their functionalized derivatives, are quite light materials (the densest

dx.doi.org/10.1021/la500111a | Langmuir 2014, 30, 4147−4156

member, Pyr-NHCH2-PAF(100%), is below 0.8 g/cm^3), we believe that volumetric uptakes are more indicative. Likely, the additional weight of a container filled by some of these adsorbents would not be a serious issue, as compared to the possibility to reduce the total volume with the same gas loading, or rather store much more gas at the same pressure.

In conclusion, the results discussed above show that functionalized PAFs, especially Pyr-NH-PAF and Pyr-NHCH2-PAF at high substitution degree, are the most promising materials for applications at low or atmospheric pressure (for instance, postcombustion CO_2 separation and capture), while at high pressures (as required, for instance, in massive gas storage) unmodified PAF-302 is preferable. A very good compromise is represented by NH2-CH2-PAF at high substitution degree, whose performance is close to the best in the whole pressure range.

6. CONCLUSIONS

The adsorption of CO_2 in different materials belonging to the PAF family has been modeled with GCMC simulations, to evaluate the performance of these materials in gas capture and storage, at different temperatures and in a wide pressure range (0−60 bar). A modified version of Dreiding force field was adopted. The Lennard-Jones parameters used for the calculation of gas−gas and gas−solid van der Waals interactions were modified, to reproduce the experimental density of the gas in the whole pressure range and to match high level quantum mechanical calculations on model systems. Throughout this Article, the difference between fugacity and pressure was properly taken into account.

Initially, four PAF-30*n* values were considered (*n* = 1−4 being the number of phenyl rings connecting the sp^3 carbons in the diamond-like structure). All of the materials are predicted to adsorb CO_2 very efficiently, with densities much higher than the compressed gas at all of the pressures. At very low pressure the best performing material is PAF-301, whose small pores and relatively high density of aromatic groups enhance the gas−surface interactions; however, PAF-301 saturates below 1 bar, and for higher pressures it is outperformed by PAF-302, which shows the best combination of specific area and microporosity. At 40 bar and 298 K (the conditions suggested by the U.S. Department of Energy for evaluating CO_2 adsorbers),[55] PAF-302 effective uptake is predicted as high as 660 mg/cm^3, corresponding to 2100 mg/g, one of the highest uptakes reported so far.

Even better results can be obtained by a suitable functionalization of PAF-302; different chemical groups, which can be actually included in PAF synthesis, have been tested to find the most promising ones and support the synthetic efforts. Also, the degree of functionalization has been considered, modeling materials with 25%, 50%, and 100% substituted phenyl rings. The results show that functionalized PAF-302 improves the CO_2 uptake dramatically at low pressure. The most efficient functional group is pyrimidine, especially using −NH− linker, which increases the adsorbed gas density at 1 bar by 2.5, 6.7, and 10.5 at 25%, 50%, and 100% substitution degree, respectively. On the other hand, at higher pressures the larger porous volume of unmodified PAF-302 becomes determinant, and the latter material provides the best performance; however, NH2-CH2-PAF, especially at high substitution degree, proved almost as efficient as PAF-302.

In summary, we believe that PAF-302 and functionalized PAF-302 are extremely promising materials for CO_2 capture and storage; among the different functional groups, pyrimidine is predicted to provide the highest uptakes at low and atmospheric pressure, while unmodified PAF-302 is expected to be the most efficient at high pressure. A very good compromise can be NH2-CH2-PAF, performing well in the whole pressure range.

■ ASSOCIATED CONTENT

Supporting Information

Table of structural data (among which density, porous volume, and specific surface area) for all of the simulated materials; modified force field Lennard-Jones parameters; PAF-30*n* unit cell models; comparison of experimental and simulated free gas densities, with standard and modified force fields; comparison of FF and ab initio energies along rigid scans for $CO_2\cdots CO_2$ and $CO_2\cdots$R−Ph (R = H, CH_3, NH_2CH_2, imidazole, pyrimidine); excess and effective adsorption isotherms for PAF-30*n* at 298 K; absolute, excess, and effective adsorption isotherms for PAF-30*n* at 273 and 323 K; comparison between experimental and simulated gravimetric adsorption in PAF-302 at 273 K; isosteric heat for PAF-30*n*; gravimetric adsorption isotherms for 25%, 50%, and 100% substituted PAF-302 at low and high pressure. This material is available free of charge via the Internet at http://pubs.acs.org.

■ AUTHOR INFORMATION

Corresponding Author

*E-mail: maurizio.cossi@mfn.unipmn.it.

Notes

The authors declare no competing financial interest.

■ ACKNOWLEDGMENTS

This work has been greatly helped by discussions with our colleagues at the Dipartimento di Scienze e Innovazione Tecnologica (University of Piemonte Orientale), in particular Giorgio Gatti, Mina Errahali, Lorenzo Tei, and Gabriele Rolla. The financial support provided by OMB-Saleri and SOL-Group is gratefully acknowledged.

■ REFERENCES

(1) Mandil, C. *World Energy Outlook*; International Energy Agency: Paris, 2006.

(2) Samanta, A.; Zhao, A.; Shimizu, G. K. H.; Sarkar, P.; Gupta, R. Post-Combustion CO2 Capture Using Solid Sorbents: A Review. *Ind. Eng. Chem. Res.* **2012**, *51*, 1438−1463.

(3) Comotti, A.; Fraccarollo, A.; Bracco, S.; Beretta, M.; Distefano, G.; Cossi, M.; Marchese, L.; Riccardi, C.; Sozzani, P. Porous Dipeptide Crystals as Selective CO2 Adsorbents: Experimental Isotherms vs. Grand Canonical Monte Carlo Simulations and MAS NMR Spectroscopy. *CrystEngComm* **2013**, *15*, 1503−1507.

(4) Cao, D.; Zhang, X.; Chen, J.; Wang, W.; Yun, J. Optimization of Single-Walled Carbon Nanotube Arrays for Methane Storage at Room Temperature. *J. Phys. Chem. B* **2003**, *107*, 13286−13292.

(5) Shao, X.; Feng, Z.; Xue, R.; Ma, C.; Wang, W.; Peng, X.; Cao, D. Adsorption of CO2, CH4, CO2/N2 and CO2/CH4 in Novel Activated Carbon Beads: Preparation, Measurements and Simulation. *AlChE J.* **2011**, *57*, 3042−3051.

(6) Hudson, M. R.; Queen, W. L.; Mason, J. A.; Fickel, D. W.; Lobo, R. F.; Brown, C. M. Unconventional, Highly Selective CO2 Adsorption in Zeolite SSZ-13. *J. Am. Chem. Soc.* **2012**, *134*, 1970−1973.

(7) Furukawa, H.; Ko, N. Ultrahigh Porosity in Metal-Organic Frameworks. *Science* **2010**, *329*, 424−428.

(8) Xiang, Z.; Hu, Z.; Cao, D.; Yang, W. T.; Lu, J.; Han, B.; Wang, W. Metal-Organic Frameworks with Incorporated Carbon Nanotubes: Improving Carbon Dioxide and Methane Storage Capacities by Lithium Doping. *Angew. Chem., Int. Ed.* **2011**, *50*, 491−494.
(9) Deng, H.; Grunder, S.; Cordova, K. E.; Valente, C.; Furukawa, H.; Hmadeh, M.; Gándara, F.; Whalley, A. C.; Liu, Z.; Asahina, S.; Kazumori, H.; O'Keeffe, M.; Terasaki, O.; Stoddart, J. F.; Yaghi, O. M. Large-Pore Apertures in a Series of Metal-Organic Frameworks. *Science* **2012**, *336*, 1018−1023.
(10) Mastalerz, M. The Next Generation of Shape-Persistant Zeolite Analogues: Covalent Organic Frameworks. *Angew. Chem., Int. Ed.* **2008**, *47*, 445−447.
(11) Battisti, A.; Taioli, S.; Garberoglio, G. Zeolitic Imidazolate Frameworks for Separation of Binary Mixtures of CO2, CH4, N-2 and H-2: A Computer Simulation Investigation. *Microporous Mesoporous Mater.* **2011**, *143*, 46−53.
(12) Ben, T.; Ren, H.; Ma, S.; Cao, D.; Lan, J.; Jing, X.; Wang, W.; Xu, J.; Deng, F.; Simmons, J. M.; Qiu, S.; Zhu, G. Targeted Synthesis of a Porous Aromatic Framework with High Stability and Exceptionally High Surface Area. *Angew. Chem., Int. Ed.* **2009**, *48*, 9457−9460.
(13) Lin, L.-C.; Berger, A. H.; Martin, R. L.; Kim, J.; Swisher, J. A.; Jariwala, K.; Rycroft, C. H.; Bhown, A. S.; Deem, M. W.; Haranczyk, M.; Smit, B. In Silico Screening of Carbon-Capture Materials. *Nat. Mater.* **2012**, *11*, 633−641.
(14) Zheng, C.; Zhong, C. Estimation of Framework Charges in Covalent Organic Frameworks Using Connectivity-Based Atom Contribution Method. *J. Phys. Chem. C* **2010**, *114*, 9945−9951.
(15) Xu, Q.; Zhong, C. A General Approach for Estimating Framework Charges in Metal-Organic Frameworks. *J. Phys. Chem. C* **2010**, *114*, 5035−5042.
(16) Amirjalayer, S.; Snurr, R. Q.; Schmid, R. Prediction of Structure and Properties of Boron-Based Covalent Organic Frameworks by a First-Principles Derived Force Field. *J. Phys. Chem. C* **2012**, *116*, 4921−4929.
(17) Ren, H.; Ben, T.; Sun, F.; Guo, M.; Jing, X.; Ma, H.; Cai, K.; Qiu, S.; Zhu, G. Synthesis of a Porous Aromatic Framework for Adsorbing Organic Pollutants Application. *J. Mater. Chem.* **2011**, *21*, 10348−10353.
(18) Ben, T.; Pei, C.; Zhang, D.; Xu, J.; Deng, F.; Jing, X.; Qiu, S. Gas Storage in Porous Aromatic Frameworks (PAFs). *Energy Environ. Sci.* **2011**, *4*, 3991−3999.
(19) Ren, H.; Ben, T.; Wang, E.; Jing, X.; Xue, M.; Liu, B.; Cui, Y.; Qiu, S.; Zhu, G. Targeted Synthesis of a 3D Porous Aromatic Framework for Selective Sorption of Benzene. *Chem. Commun.* **2010**, *46*, 291−293.
(20) Yuan, Y.; Sun, F.; Ren, H.; Jing, X.; Wang, W.; Ma, H.; Zhao, H.; Zhu, G. Targeted Synthesis of a Porous Aromatic Framework with a High Adsorption Capacity for Organic Molecules. *J. Mater. Chem.* **2011**, *21*, 13498−13502.
(21) Lan, J.; Cao, D.; Wang, W.; Ben, T.; Zhu, G. High-Capacity Hydrogen Storage in Porous Aromatic Frameworks with Diamond-like Structure. *J. Phys. Chem. Lett.* **2010**, *1*, 978−981.
(22) Babarao, R.; Dai, S.; Jiang, J. Functionalizing Porous Aromatic Frameworks with Polar Organic Groups for High-Capacity and Selective CO2 Separation: A Molecular Simulation Study. *Langmuir* **2011**, *27*, 3451−3460.
(23) Li, Y.; Ben, T.; Zhang, B.; Fu, Y.; Qiu, S. Ultrahigh Gas Storage both at Low and High Pressures in KOH-Activated Carbonized Porous Aromatic Frameworks. *Sci. Rep.* **2013**, *3*, 1−6.
(24) Ben, T.; Li, Y.; Zhu, L.; Zhang, D.; Cao, D.; Xiang, Z.; Yao, X.; Qiu, S. Selective Adsorption of Carbon Dioxide by Carbonized Porous Aromatic Framework (PAF). *Energy Environ. Sci.* **2012**, *5*, 8370−8376.
(25) Konstas, K.; Taylor, J. W.; Thornton, A. W.; Doherty, C. M.; Lim, W. X.; Bastow, T. J.; Kennedy, D. F.; Wood, C. D.; Cox, B. J.; Hill, J. M.; Hill, A. J.; Hill, M. R. Lithiated Porous Aromatic Frameworks with Exceptional Gas Storage Capacity. *Angew. Chem., Int. Ed.* **2012**, *51*, 1−5.
(26) Ma, H.; Ren, H.; Zou, X.; Sun, F.; Yan, Z.; Cai, K.; Wang, D.; Zhu, G. Novel Lithium-Loaded Porous Aromatic Framework for Efficient CO2 and H-2 Uptake. *J. Mater. Chem. A* **2013**, *1*, 752−758.
(27) Lu, W.; Yuan, D.; Sculley, J.; Zhao, D.; Krishna, R.; Zhou, H.-C. Sulfonate-Grafted Porous Polymer Networks for Preferential CO2 Adsorption at Low Pressure. *J. Am. Chem. Soc.* **2011**, *133*, 18126−18129.
(28) Trewin, A.; Cooper, A. Porous Organic Polymers: Distinction from Disorder? *Angew. Chem., Int. Ed.* **2010**, *49*, 1533−1535.
(29) Yuan, D.; Lu, W.; Zhao, D.; Zhou, H. C. Highly Stable Porous Polymer Networks with Exceptionally High Gas-Uptake Capacities. *Adv. Mater.* **2011**, *23*, 3723−3725.
(30) Yang, Z.; Peng, X.; Cao, D. Carbon Dioxide Capture by PAFs and an Efficient Strategy To Fast Screen Porous Materials for Gas Separation. *J. Phys. Chem. C* **2013**, *117*, 8353−8364.
(31) *Materials Studio 6.0*; Accelrys Software Inc.: San Diego, CA, 2011.
(32) Frenkel, D.; Smith, B. *Understanding Molecular Simulations*; Academic Press: New York, 2002.
(33) Becke, A. D. A New Mixing of Hartree-Fock and Local Density-Functional Theories. *J. Chem. Phys.* **1993**, *98*, 1372−1377.
(34) Hariharan, P. C.; Pople, J. A. Influence of Polarization Functions on Molecular-Orbital Hydrogenation Energies. *Theor. Chim. Acta* **1973**, *28*, 213−222.
(35) Clark, T.; Chandrasekhar, J.; Spitznagel, G. W.; Schleyer, P. v. R. Efficient Diffuse Function-Augmented Basis Sets for Anion Calculations. III. The 3-21+G Basis Set for First-Row Elements, Li-F. *J. Comput. Chem.* **1983**, *4*, 294−301.
(36) Dovesi, R.; Saunders, V. R.; Roetti, C.; Orlando, R.; Zicovich-Wilson, C. M.; Pascale, F.; Civalleri, B.; Doll, K.; Harrison, N. M.; Bush, I. J.; D'Arco, P.; Llunell, M. *CRYSTAL09 User's Manual*; University of Torino: Torino, 2013.
(37) Boys, S. F.; Bernardi, F. Calculation of Small Molecular Interactions by Differences of Separate Total Energies - Some Procedures with Reduced Errors. *Mol. Phys.* **1970**, *19*, 553−566.
(38) Frisch, M. J.; Trucks, G. W.; Schlegel, H. B.; Scuseria, G. E.; Robb, M. A.; Cheeseman, J. R.; Scalmani, G.; Barone, V.; Mennucci, B.; Petersson, G. A.; Nakatsuji, H.; Caricato, M.; Li, X.; Hratchian, H. P.; Izmaylov, A. F.; Bloino, J.; Zheng, G.; Sonnenberg, J. L.; Hada, M.; Ehara, M.; Toyota, K.; Fukuda, R.; Hasegawa, J.; Ishida, M.; Nakajima, T.; Honda, Y.; Kitao, O.; Nakai, H.; Vreven, T.; Montgomery, J. A., Jr.; Peralta, J. E.; Ogliaro, F.; Bearpark, M.; Heyd, J. J.; Brothers, E.; Kudin, K. N.; Staroverov, V. N.; Kobayashi, R.; Normand, J.; Raghavachari, K.; Rendell, A.; Burant, J. C.; Iyengar, S. S.; Tomasi, J.; Cossi, M.; Rega, N.; Millam, N. J.; Klene, M.; Knox, J. E.; Cross, J. B.; Bakken, V.; Adamo, C.; Jaramillo, J.; Gomperts, R.; Stratmann, R. E.; Yazyev, O.; Austin, A. J.; Cammi, R.; Pomelli, C.; Ochterski, J. W.; Martin, R. L.; Morokuma, K.; Zakrzewski, V. G.; Voth, G. A.; Salvador, P.; Dannenberg, J. J.; Dapprich, S.; Daniels, A. D.; Farkas, Ö.; Foresman, J. B.; Ortiz, J. V.; Cioslowski, J.; Fox, D. J. *Gaussian 09*, revision D; Gaussian, Inc.: Pittsburgh, PA, 2009.
(39) Lemmon, E. W.; McLinden, M. O.; Friend, D. G. *NIST Chemistry WebBook Nist standard reference database number 69*; National Institute of Standards and Technology: Washington, DC, 2011.
(40) Span, U.; Wagner, W. A New Equation of State for Carbon Dioxide. *J. Phys. Chem. Ref. Data* **1996**, *25*, 1509−1596.
(41) Cossi, M.; Gatti, G.; Canti, L.; Errahali, M.; Tei, L.; Marchese, L. Theoretical Prediction of High Pressure Methane Adsorption in Porous Aromatic Frameworks (PAFs). *Langmuir* **2012**, *28*, 14405−14414.
(42) Garibay, S. J.; Weston, M. H.; Mondloch, J. E.; Colon, Y. J.; Farha, O. K.; Hupp, T. H.; Nguyen, S. T. Accessing Functionalized Porous Aromatic Frameworks (PAFs) through a De Novo Approach. *CrystEngComm* **2013**, *15*, 1515−1519.
(43) Couck, S.; Denayer, J. F. M.; Baron, G. V.; Remy, T.; Gascon, J.; Kapteijn, F. An Amine-Functionalized MIL-53 Metal-Organic Framework with Large Separation Power for CO_2 and CH_4. *J. Am. Chem. Soc.* **2009**, *131*, 6326−6327.

(44) Torrisi, A.; Bell, R. G.; Mellot-Draznieks, C. Functionalized MOFs for Enhanced CO_2 Capture. *Cryst. Growth Des.* **2010**, *10*, 2839−2841.
(45) Pascual-Ahuir, J.-L.; Silla, E.; Tuñon, I. GEPOL - An Improved Description of Molecular-Surfaces 0.3. A New Algorithm for the Computation of a Solvent-Excluding Surface. *J. Comput. Chem.* **1994**, *15*, 1127−1138.
(46) Barone, V.; Cossi, M.; Tomasi, J. A New Definition of Cavities for the Computation of Solvation Free Energies by the Polarizable Continuum Model. *J. Chem. Phys.* **1997**, *107*, 3210−3221.
(47) Mayo, S. L.; Olafson, B. D.; Goddard, W. A. Dreiding - A Generic Force-Field for Molecular Simulations. *J. Phys. Chem.* **1990**, *94*, 8897−8909.
(48) Düren, T.; Bae, Y. S.; Snurr, R. Q. Using Molecular Simulation to Characterise Metal-Organic Frameworks for Adsorption Applications. *Chem. Soc. Rev.* **2009**, *38*, 1237−1247.
(49) Li, Y.; Yang, R. T. Gas Adsorption and Storage in Metal-Organic Framework MOF-177. *Langmuir* **2007**, *23*, 12937−12944.
(50) Kaye, S. S.; Dailly, A.; Yaghi, O. M.; Long, J. R. Impact of Preparation and Handling on the Hydrogen Storage Properties of Zn_4O(1,4−benzenedicarboxylate)$_3$ (MOF-5). *J. Am. Chem. Soc.* **2007**, *129*, 14176−14177.
(51) Wade, C. R.; Corrales-Sanchez, T.; Narayan, T. C.; Dincă, M. Postsynthetic Tuning of Hydrophilicity in Pyrazolate MOFs To Modulate Water Adsorption Properties. *Energy Environ. Sci.* **2013**, *6*, 2172−2177.
(52) Jasuja, H.; Walton, K. S. Effect of Catenation and Basicity of Pillared Ligands on the Water Stability of MOFs. *Dalton Trans.* **2013**, *42*, 15421−15426.
(53) Furukawa, H.; Yaghi, O. M. Storage of Hydrogen, Methane, and Carbon Dioxide in Highly Porous Covalent Organic Frameworks for Clean Energy Applications. *J. Am. Chem. Soc.* **2009**, *131*, 8875−8883.
(54) Zheng, B.; Yun, R.; Bai, J.; Lu, Z.; Du, L.; Li, Y. Expanded Porous MOF-505 Analogue Exhibiting Large Hydrogen Storage Capacity and Selective Carbon Dioxide Adsorption. *Inorg. Chem.* **2013**, *52*, 2823−2829.
(55) *Advanced Carbon Dioxide Capture R&D Program: Technology Update*; National Energy Technology Laboratory, DOE, 2011.